Sensors and Materials, Vol. 15, No. 3 (2003) 113–135
MYU Tokyo

S & M 0514

Silicon Piezoresistive Six-Degree of Freedom Force-Moment Micro Sensor

Dzung Viet Dao, Toshiyuki Toriyama[1], John Wells and Susumu Sugiyama

Graduate School of Science and Engineering, Ritsumeikan University
1-1-1 Noji-Higashi, Kusatsu, Shiga 525-8577, Japan
[1]New Energy and Industrial Technology Development Organaization
Higashi-Ikebukuro, Toshima-Ku, Tokyo 170-6028, Japan

(Received May 27, 2002; accepted February 20, 2003)

Key words: piezoresistance effect, micro force-moment sensor, 6 degrees of freedom, FEM analysis

In this paper, we describe the design, fabrication and calibration results of a 6-degree of freedom force-moment micro sensing chip utilizing the piezoresistance effect in silicon. The sensing chip is designed to be able to simultaneously detect three components of force and three components of moment in three orthogonal directions. Conventional p-type and four-terminal p-type piezoresistors have been combined in this single sensing chip in the (111) plane of silicon. The total number of piezoresistors is 18, much fewer than the previous piezoresistance-based 6-component force moment sensors known to the authors. Calibration results show linear output responses (the maximum nonlinearity is 2% F.S.), and small crosstalk (the maximum crosstalk is less than 4%). The immediate purpose of the sensing chip development is to measure the forces and moments acting on boundary particles in a turbulent liquid flow. The configuration of the turbulent flow sensor and the preliminary results of an experiment in a water channel are presented.

1. Introduction

Recently, the demands for micro force sensors in engineering applications are increasing. There have been substantial research and fabrication efforts for micro force sensors. Some examples of these are the three-component force sensors,[1,2] normal force sensor,[3] shear force sensor,[4] and three-dimensional tactile sensors.[5,6] While much work has dealt with three-component force sensors, studies on six force-moment components micro sensors are rare. The three-component sensors are adequate for the tasks involving feature identification, or determining object location. However, for certain applications, they are

*Corresponding author, e-mail address: ddv99212@se.ritsumei.ac.jp

inadequate.[7] Examples of such applications include measuring external forces on particles in liquid flows, and grasping and manipulation by a robot hand. There have been several approaches to the design and fabrication of full six-component force sensors. Sinden and Boie[8] introduced some theoretical designs of a planar capacitive force sensor with six degrees of freedom (6-DOF). However, these designs are more complex than those of piezoresistance sensors and not economical to fabricate with MEMS in terms of fabrication accuracy, reproducibility, and sensor dimension. Some centimeter-scale conventional 6-DOF force sensors have also been presented,[9,10] in which the metallic strain gauges were fixed on a spatial structure. Kim *et al.*[11] designed and fabricated a six-component force moment sensor, which used a crossbeam combined with eight other surrounding beams for measuring *Fx, Fy, Fz, Mx, My* and *Mz*. Twenty-four strain gages were bonded on the surfaces of the beams. These sensors are large and structurally complicated. Grahn[7] invented a triaxial normal and shear force sensor, which used the ultrasonic technique as the detecting principle. Okada[12] also reported a planar six-axis force sensor based on the silicon piezoresistance effect. Forty-eight piezoresistors are formed at twenty-four locations on the upper surface of beams. This structure, then, was bonded on the surface of a strain generative body. Large numbers of piezoresistors on beams make the electrical circuit complicated, and result in high power dissipation, wide beams, and consequently, high structural stiffness. Maximum crosstalk of about 24% was reported. Jin and Mote[13] developed a six-component silicon micro force sensor. Lorentz forces were used to calibrate the sensor. However, eight Wheatstone bridges were arranged on the four diaphragms increasing the size of the sensing area, or in other words, increasing the structural stiffness. Furthermore, the assembling of three components made the sensor sophisticated and larger in overall size. Crosstalk above 10% was reported.

In this research, a piezoresistance-based micro sensing chip with 6-DOF using only 16 conventional and two four-terminal piezoresistors is described. The sensing chip presented in this paper was designed for application to the measurement of turbulent flow, and design ranges of force and moment were based on the estimated fluid forces.[14,15] Unlike other flow sensors, which typically measure just one component of wall shear stress,[16,17] the proposed sensor can independently detect six components of force and moment on a test particle in a turbulent flow. The structural analysis was carried out by FEM to optimize the dimensions and to locate the optimal positions for the piezoresistors. Then, the sensing chip was fabricated by micromachining processes. Finally, the sensing chip was calibrated using a computer-controlled ultra-small load indenter. A specific configuration of the sensor to measure forces and moments acting on a test particle in turbulent liquid flows, as well as preliminary experimental results are also briefly presented.

Although the design of the sensing chip is illustrated hereafter referring to a turbulent flow sensor, extension to other integrated force-based micro devices, such as tactile sensors, and micro multi-axis accelerometers is straightforward.

2. Design of Sensing Chip

The sensing chip is a single crystalline silicon crossbeam with two-terminal (conventional type) and four-terminal piezoresistors diffused on the surface of the four suspended-beams. Forces and moments applied to the sensing chip, shown in Fig. 1, deform the four

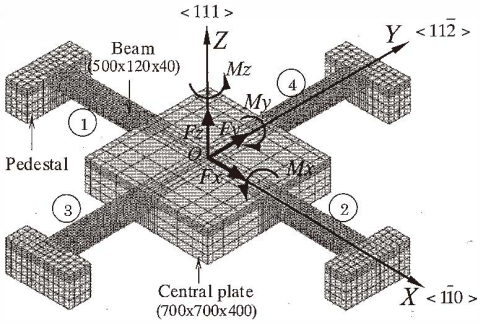

Fig. 1. FEM model of sensing chip (unit: μm).

suspended-beams and change the resistance of the piezoresistors, which leads to a change in output of corresponding measurement circuits. The beam's size, piezoresistance coefficients and the positions of piezoresistors on the sensing chip are the main factors determining the sensitivity of the sensor. This section discusses how crystallographic orientations and piezoresistor arrangement were specified in order to obtain large sensitivity while satisfying the constraint that the sensor can detect six components of force and moment independently.

2.1 *Piezoresistance effect—selection of crystallographic orientations*

The piezoresistance effect is a phenomenon in which the electrical resistivity of a material changes due to applied stress. In semiconductors, strain-induced distortions of the energy band structure affect the mobility of the electrons and holes, and also redistribute the electron and hole concentrations. These changes in turn lead to the change of electrical resistivity ρ of the semiconductor. Substantial calculations of piezoresistance coefficients in single crystal silicon have been performed here recently,[18,19] valuable results have been obtained. In this research, forces and moments are measured by two-terminal (conventional type) and four-terminal piezoresistors. The piezoresistance effect of conventional piezoresistors can be expressed as[20]

$$\frac{\Delta R}{R} = \pi'_{11}\sigma_1 + \pi'_{12}\sigma_2 + \pi'_{13}\sigma_3 + \pi'_{14}\tau_4 + \pi'_{15}\tau_5 + \pi'_{16}\tau_6, \tag{1}$$

where $\frac{\Delta R}{R}$ is the relative change of resistance due to the normal stresses σ_i (i = 1, 2, 3), and shear stresses τ_j (j = 4, 5, 6). The primed quantities π'_{1k}, (k = 1, 2, 3, 4, 5 and 6), are the piezoresistance coefficients referred to arbitrarily oriented axes, or to a Cartesian system: 1′, 2′, and 3′. These coefficients π'_{1k}, being derived from fourth-rank tensor, originally have four subscripts, of which the first refers to the electrical field direction, the second to the current density direction, and the last two to the stress component involved. In eq. (1), each subscript of π'_{1j} has been substituted for two of the original four subscripts according

to the subscript-transformation scheme: 11→1, 22→2, 33→3, 23 = 32→4, 31 = 13→5, 12 = 21→6. Here, the first subscript of π'_{1k} equals 1, because in the case of a two-terminal piezoresistor, the electrical current and electrical field are in the same direction, which is conventionally aligned with axis 1′. Each subscript of σ_i (i= 1, 2, 3), τ_j (j = 4, 5, 6), and the second subscript of π'_{1k}, (k=1, 2, 3, 4, 5, 6) have been substituted for two original subscripts, which represent the two indices of the stress tensor, by the same subscript-transformation scheme mentioned above. In eq. (1), the resistance change due to the effects of dimensional changes (usually two orders smaller than the resistance change due to resistivity change[21]) was ignored. The piezoresistance coefficients depend on material, temperature, and orientation. The piezoresistance coefficients π'_{1j} can be expressed as functions of the orientations and the fundamental piezoresistance coefficients of the cubic single crystalline silicon, *i.e.*, π_{11}, π_{12}, π_{44}, as[20]

$$\pi'_{11} = \pi_{11} - 2(\pi_{11} - \pi_{12} - \pi_{44})\left[(l_1 m_1)^2 + (n_1 m_1)^2 + (l_1 n_1)^2\right], \tag{2}$$

$$\pi'_{12} = \pi_{12} + (\pi_{11} - \pi_{12} - \pi_{44})\left[(l_1 l_2)^2 + (m_1 m_2)^2 + (n_1 n_2)^2\right], \tag{3}$$

$$\pi'_{13} = \pi_{12} + (\pi_{11} - \pi_{12} - \pi_{44})\left[(l_1 l_3)^2 + (m_1 m_3)^2 + (n_1 n_3)^2\right], \tag{4}$$

$$\pi'_{14} = 2(\pi_{11} - \pi_{12} - \pi_{44})(l_1^2 l_2 l_3 + m_1^2 m_2 m_3 + n_1^2 n_2 n_3), \tag{5}$$

$$\pi'_{15} = 2(\pi_{11} - \pi_{12} - \pi_{44})(l_1^3 l_3 + m_1^3 m_3 + n_1^3 n_3), \tag{6}$$

$$\pi'_{16} = 2(\pi_{11} - \pi_{12} - \pi_{44})(l_1^3 l_2 + m_1^3 m_2 + n_1^3 n_2). \tag{7}$$

That is, the 1′-axis has the direction cosines l_1, m_1, n_1, the 2′-axis has the direction cosines l_2, m_2, n_2, and the 3′-axis has the direction cosines l_3, m_3, n_3 with respect to the principal crystallographic axes 1, 2 and 3, respectively. These direction cosines can be calculated through Euler's angles in the transformation of the coordinate system from principal crystallographic axes to the considered directions. π_{11}, π_{12} and π_{44} are the fundamental piezoresistance coefficients of the cubic single crystal. For a bulk p-type piezoresistor with a resistivity of 7.8 Ω cm, these coefficients are $\pi_{11} = 6.6 \times 10^{-11}$ Pa^{-1}, $\pi_{12} = -1.1 \times 10^{-11}$ Pa^{-1} and $\pi_{44} = 138.1 \times 10^{-11}$ Pa^{-1}.[22] In fact, the piezoresistance coefficients of the diffused layer depend on impurity concentration and are much smaller than these bulk values. With an impurity concentration of about 5×10^{19} cm^{-3} (typical of our process), $\pi_{11} = 1.5 \times 10^{-11}$ Pa^{-1}, $\pi_{44} = 85 \times 10^{-11}$ Pa^{-1}.[23]

In a four-terminal piezoresistor, on the other hand, normal and shear stresses can produce an electrical field that is perpendicular to the direction of current flow.[20,24] If one ignores extremely small effects of dimensional changes, the output transverse voltage between two voltage traps V_{out} of a four-terminal piezoresistor can be expressed as:

$$\frac{V_{out}}{V_{in}} = \pi'_{61}\sigma_1 + \pi'_{62}\sigma_2 + \pi'_{63}\sigma_3 + \pi'_{64}\tau_4 + \pi'_{65}\tau_5 + \pi'_{66}\tau_6. \tag{8}$$

Here, V_{in} is the supply voltage, and the primed quantities π'_{6i} (i=1, 2, 3, 4, 5 and 6), are the piezoresistance coefficients corresponding to normal and shear stresses of a four-terminal piezoresistor in arbitrary orientations. The coefficients π'_{6i} are derived from a fourth-rank tensor by the transformation rule employed for π'_{1i} mentioned above. The first subscript is 6 implying that the current density component and electrical field component are in perpendicular directions, *i.e.,* 1′ and 2′. π'_{6i} can be expressed in terms of direction cosines and fundamental piezoresistance coefficients π_{11}, π_{12} and π_{44}, as:

$$\pi'_{61} = (\pi_{11} - \pi_{12} - \pi_{44})(l_1^3 l_2 + m_1^3 m_2 + n_1^3 n_2), \tag{9}$$

$$\pi'_{62} = (\pi_{11} - \pi_{12} - \pi_{44})(l_1 l_2^3 + m_1 m_2^3 + n_1 n_2^3), \tag{10}$$

$$\pi'_{63} = (\pi_{11} - \pi_{12} - \pi_{44})(l_1 l_2 l_3^2 + m_1 m_2 m_3^2 + n_1 n_2 n_3^2), \tag{11}$$

$$\pi'_{64} = 2(\pi_{11} - \pi_{12} - \pi_{44})(l_1 l_2^2 l_3 + m_1 m_2^2 m_3 + n_1 n_2^2 n_3), \tag{12}$$

$$\pi'_{65} = 2(\pi_{11} - \pi_{12} - \pi_{44})(l_1^2 l_2 l_3 + m_1^2 m_2 m_3 + n_1^2 n_2 n_3), \tag{13}$$

$$\pi'_{66} = \pi_{44} + 2(\pi_{11} - \pi_{12} - \pi_{44})(l_1^2 l_2^2 + m_1^2 m_2^2 + n_1^2 n_2^2). \tag{14}$$

The coefficients π'_{1i}, and π'_{6i} (i = 1, 2, 3, 4, 5, 6), can be made large or small by selecting suitable orientations, *i.e.,* changing the direction cosines l_j, m_j, n_j (j = 1, 2, 3) in eqs. (1) – (7) and (9) – (14). For convenience, we will assume that the *X*-axis, *Y*-axis, *Z*-axis (Fig. 1) are aligned with 1′, 2′ and 3′, respectively.

In our research, the piezoresistors are formed by the mask-diffusion method, so the piezoresistors lie on the surface of the sensing beams, and are very thin in comparison with the thickness of the beams. Stress analysis on the surface of a sensing structure, which will be presented in section 2.2, shows that the components σ_1 (the tensile or compressive stress components parallel to direction 1′ (*X*-axis) or 2′ (*Y*-axis)) and τ_6 (the shear stress component in the plane containing axes 1′ and 2′, called in-plane shear stress") are found to be much larger than other components of stress, and become dominant for sensing purposes. For this reason, one of the criteria to select the crystallographic orientation is to make π'_{11} and π'_{66} as large as possible. Investigating various crystallographic orientations of single crystal silicon, the two crystallographic orientations, $<1\bar{1}0>$ and $<11\bar{2}>$ of silicon (111), were chosen to be the in-plane principal axes of the piezoresistors, since these orientations meet the selection criteria mentioned above, and the silicon (111) wafers are widely available on the market.

Substituting the direction cosines of these directions ($<1\bar{1}0>$, $<11\bar{2}>$ and $<111>$) with respect to the principal crystallographic orientations ($<100>$, $<010>$ and $<001>$) into eqs. (1) – (7) and (9) – (14), we have:

$$\pi'_{11} = \frac{1}{2}(\pi_{11} + \pi_{12} + \pi_{44}),\ \pi'_{12} = \frac{1}{6}(\pi_{11} + 5\pi_{12} - \pi_{44}),\ \pi'_{13} = \frac{1}{3}(\pi_{11} + 2\pi_{12} - \pi_{44}),$$

$$\pi'_{14} = \frac{\sqrt{2}}{3}(\pi_{11} - \pi_{12} - \pi_{44}),\ \pi'_{15} = 0,\ \pi'_{16} = 0,$$
$$\pi'_{61} = 0, \pi'_{62} = 0,\ \pi'_{63} = 0,\ \pi'_{64} = 0,$$
$$\pi'_{65} = \frac{\sqrt{2}}{3}(\pi_{11} - \pi_{12} - \pi_{44}),\ \pi'_{66} = \frac{1}{3}(\pi_{11} - \pi_{12} + 2\pi_{44}).$$

Equations (1) and (8) can be rewritten as:

$$\frac{\Delta R}{R} = \pi'_{11}\sigma_1 + \pi'_{12}\sigma_2 + \pi'_{13}\sigma_3 + \pi'_{14}\tau_4 + \pi'_{15}\tau_5, \tag{15}$$

$$\frac{V_{out}}{V_{in}} = \pi'_{65}\tau_5 + \pi'_{66}\tau_6. \tag{16}$$

Equation (15) implies that the two-terminal piezoresistors in these crystallographic orientation are not sensitive to in-plane shear stress, *i.e.,* the component τ_6, while eq. (16) indicates that the four-terminal piezoresistors in these orientations are not sensitive to normal stress, *i.e.,* the components σ_1, σ_2, σ_3. Hence, the four-terminal piezoresistor is named shear stress piezoresistor, or shear piezoresistor. The complementary properties of these two types of piezoresistors form the basis of our sensing principle for independently detecting in-plane shear stress and normal stress. Equations (15) and (16) can be further shortened by considering the stress distributions on the surface layer of the crossbeam, which will be described in the next section.

The selection of silicon (111) has turned out to have another advantage; π'_{11} and π'_{66} are constant in all directions in plane (111), so that the sensitivities to σ_1 and τ_6 are constant along all orientations in the plane (111).

2.2 *Structural analysis of the sensing chip and piezoresistor arrangement on the beams*

The structural analysis of the sensing chip consists of two steps. The first step deals with qualitative analysis by classical elasticity theory. The dimensions of the sensing chip were tentatively specified based on the specified ranges of force and moment acting on a test particle (diameter of 10 mm) in water flow,[14,15] and the desired sensitivity, the piezoresistance effect of silicon, the nonbuckling condition, and the necessary width of beam for wiring.

Next, this model was analyzed by a finite element method (FEM) to investigate more comprehensively the stress field in the structure, and to refine the specifications of the beam dimensions. Figure 1 shows the finite element model of the sensing chip for numerical analysis using MENTAT 3.1 software (MARC Research Corp.). The axes *X, Y, Z* are aligned with directions $<1\bar{1}0>$, $<11\bar{2}>$ and $<111>$, respectively. The dimensions of each suspended-beam of the crossbeam (length × width × thickness) are 500 × 120 × 40 μm^3. A total of 9772 hexahedral elements (MARC element class hex 8), with 13280 nodes are used to mesh the model. The model is densely meshed in the beams to better

resolve the stress distribution there. The two lateral faces of each of the four pedestals at the outer ends of beams were fixed for the boundary condition. The anisotropic elasticity of silicon (111) is taken into account during FEM analysis to obtain more reliable simulation results. To calculate stiffness coefficients of silicon in the two directions $<1\bar{1}0>$ and $<11\bar{2}>$ in plane (111), the transformation rule for the fourth-rank tensor described in section 2.1 has been used. Because of the symmetry, this fourth-rank stiffness tensor can be expressed by a 6×6 matrix notation $[C]$, by applying the subscript transformation scheme mentioned above. The coefficients of matrix $[C]$ have been calculated based on the three stiffness coefficients of principal crystallographic orientations $<100>$, $<010>$, $<001>$: $C_{11} = 1.657 \times 10^5$ MPa, $C_{12} = 0.639 \times 10^5$ MPa, $C_{44} = 0.796 \times 10^5$ MPa.[25]

$$[C'] = \begin{bmatrix} C'_{11} & C'_{12} & C'_{13} & C'_{14} & C'_{15} & C'_{16} \\ & C'_{22} & C'_{23} & C'_{24} & C'_{25} & C'_{26} \\ & & C'_{33} & C'_{34} & C'_{35} & C'_{36} \\ & \text{Symmetry} & & C'_{44} & C'_{45} & C'_{46} \\ & & & & C'_{55} & C'_{56} \\ & & & & & C'_{66} \end{bmatrix} = \begin{bmatrix} 1.944 & 0.543 & 0.447 & 0.135 & 0.000 & 0.000 \\ & 1.944 & 0.447 & -0.135 & 0.000 & 0.000 \\ & & 2.039 & 0.000 & 0.000 & 0.000 \\ & \text{Symmetry} & & 0.605 & 0.000 & 0.000 \\ & & & & 0.605 & 0.135 \\ & & & & & 0.700 \end{bmatrix} \times 10^5 \text{ MPa}$$

Figures 2 – 5 show the distributions of stress components along the central axes on the surface of *X*-oriented and *Y*-oriented beams due to the application of each force or moment applied to the central point *O* of the chip. The point *O* coincides with the center of the central plate and lies on the neutral surface of the beams. Stresses in the central plate are not indicated since this area is not used for sensing purposes. The stress component σ_1 is the normal stress component parallel to the longitudinal axis of a beam and also to the direction of current density and electrical field of the conventional piezoresistors placed on that beam. Hence, it is called longitudinal stress σ_L. The component σ_2 is the normal stress component perpendicular to the longitudinal axis of a beam and of the conventional piezoresistors placed on that beam. It is called transverse stress; σ_3 is the normal stress component perpendicular to σ_1 and σ_2; Component τ_6 is an in-plane shear stress component (*i.e.,* the shear stress component in the plane of the four-terminal piezoresistor, in this case it is the plane (*XOY*)), and τ_4, τ_5 are out-of-plane shear stress components.

Figure 2(a) shows the stress distributions along the central axes on the surface of *X*-oriented beams due to the action of a moment *My* (around the *Y* axis) applied to the central point *O* of the chip. From this figure, we can see that only the longitudinal stress component σ_1 is large, while other stress components (*i.e.,* σ_2, σ_3, τ_4, τ_5, τ_6) are so small that they can be ignored. Hence, to measure a moment *My*, conventional piezoresistors R_{My1}, R_{My2}, R_{My3}, R_{My4} are placed where the stress components σ_1 are large, *i.e.* near the fixed ends of beams ① and ②, (Fig. 2(a)). The beams ③ and ④ are twisted, so in-plane shear stresses (τ_6) of equal magnitude, but opposite sign will occur along the central line on the surface of these beams (Fig.2(b)). These stress components equal zero along the beams' edges.[26]

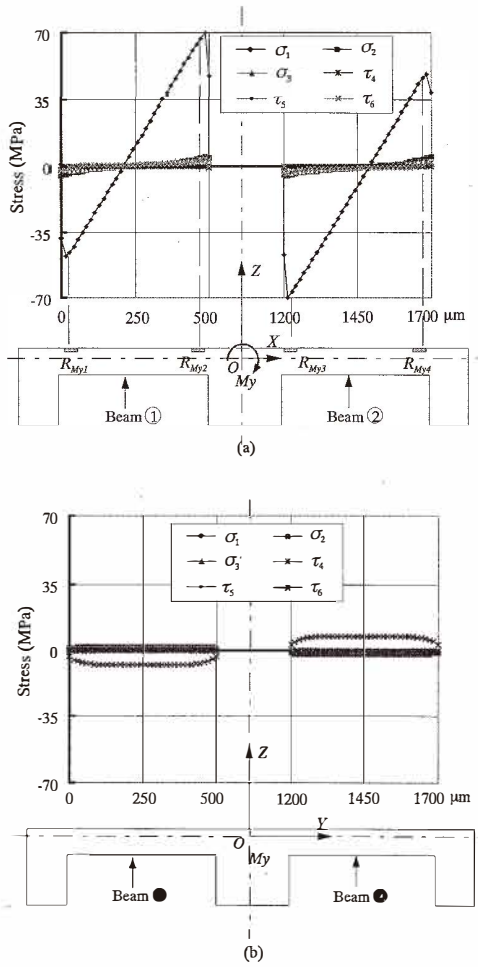

Fig. 2. Stress distributions due to a moment *My*. (a) Along central axis on the surface of *X*-oriented beams. (b) Along central axis on the surface of *Y*-oriented beams.

When a force *Fx* is applied to the central point *O* of the sensing chip (Fig. 1), the stress states in beam ① and beam ② are equivalent to the case in which a clamped-free prismatic beam is pulled or compressed, respectively. Hence, beam ① undergoes a constant compressive stress ($-\sigma_1$) along it, while beam ② undergoes a constant tensile stress (σ_1) along it.[26] Due to the symmetry of the model, these two stresses are equal in magnitude (Fig. 3(a)). To obtain high sensitivity to this force, two conventional piezoresistors R_{Fx1}, R_{Fx2} can be placed anywhere in the large stress area on each beam. The optimal positions of each piezoresistor on each beam coincide with the point, at which the stress σ_1 induced by moment *My* equals zero. The FEM results have shown that these stress-free points are

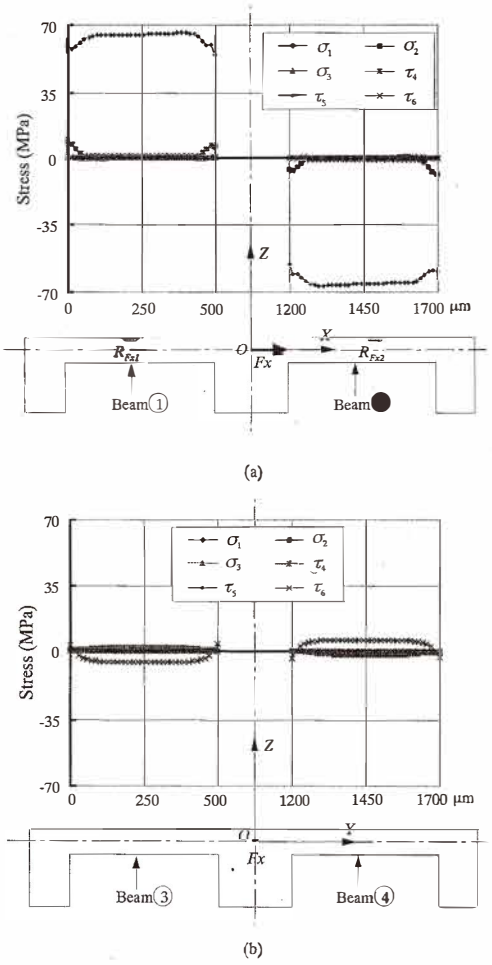

Fig. 3. Stress distributions due to a force Fx. (a) Along the central axis on the surface of X-oriented beams. (b) Along the central axis on the surface of Y-oriented beams.

unchanged when moment My is changed. Other stress components are almost zero along these beams, (Fig. 3(a)). Along the central axes on the surface of the Y-oriented beams ③ and ④, in-plane shear stresses (τ_6) with the same magnitude but opposite sign will occur (Fig. 3(b)).

In case there is a vertical force Fz acting on the central point O of the sensing chip, the stresses in four beams are similar due to the symmetry of the model. The stress distributions along the central axes on the surface of the X-oriented beams ① and ② are shown in Fig. 4. The only longitudinal stress σ_1 is large and becomes a principal stress component. Hence, to measure Fz, four conventional piezoresistors R_{Fz1}, R_{Fz2}, R_{Fz3}, R_{Fz4} are arranged near the fixed ends of beams ① and ②, because the longitudinal stresses are large there.

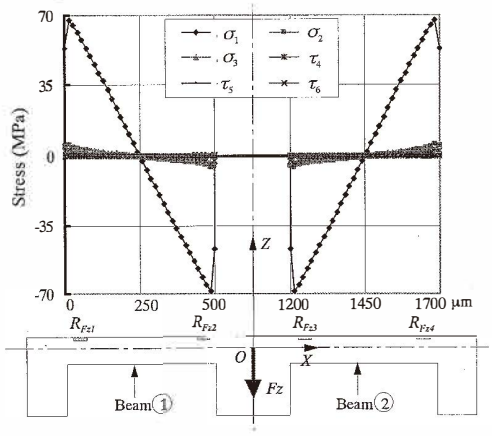

Fig. 4. Stress distributions along central axis on the surface of the *X*-oriented beams due to force *Fz*.

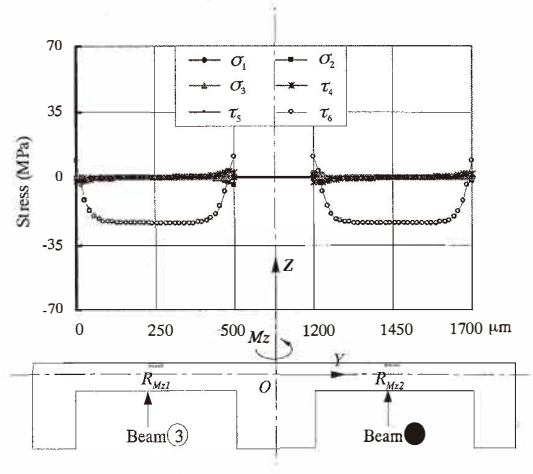

Fig. 5. Stress distributions along central axis on the surface of the *Y*-oriented beams due to *Mz*.

When a moment *Mz* (around the *Z*-axis) is applied to the central point *O* of the sensing chip, stress statuses in the four beams are similar, because of the symmetry of the model. Stress distributions along the central axis on the surface of beams ③ and ④ are shown in Fig. 5. In this case, the significant stress components are in-plane shear stresses (τ_6). Hence, to measure moment *Mz*, two shear piezoresistors R_{Mz1}, R_{Mz2} are placed, one on each beam, at positions with large in-plane shear stresses. Other stress components are nearly

zero along these lines.

From classical elasticity and the FEM analysis, the stress statuses along the central axes on the surface of the beams were completely clarified. The piezoresistors' positions on the beams were determined. Accordingly, sixteen p-type conventional piezoresistors (four piezoresistors R_{Fz}, two piezoresistors R_{Fx} and four piezoresistors R_{My} are on X-oriented beams ① and ②; two piezoresistors R_{Fy} and four piezoresistors R_{Mx}, are on Y-oriented beams ③ and ④), and two p-type shear piezoresistors (R_{Mz1} and R_{Mz2} are on Y-oriented beams ③ and ④, respectively, to measure the moment Mz), were formed by using impurity diffusion along the central-longitudinal axes on the upper surface of an n-type silicon crossbeam. Figure 6 shows the layout of all eighteen piezoresistors on the surface of the crossbeam. The piezoresistors to measure one component of force or moment were arranged symmetrically through central point O on the two beams. All conventional piezoresistors were designed to be identical, as were the two shear piezoresistors.

The structural analysis results also show that, the out-of-plane shear stress components (*i.e.*, τ_4 and τ_5) on the beams' surface are so small that they can be ignored. The transverse stress components σ_2 and σ_3 are almost two orders smaller than σ_1, except in the area adjacent to the fixed ends of the beams, where σ_2 has the same sign and is about tens times smaller than σ_1. The appearance of this stress component in piezoresistors will slightly affect the sensitivity of the sensing chip (see eq. (15) and note that π'_{11} and π'_{12} are opposite in sign). Hence, the piezoresistors have been arranged far enough from the fixed ends of beams (at least 10 μm or 2% of the beam length) to avoid this undesirable stress component.

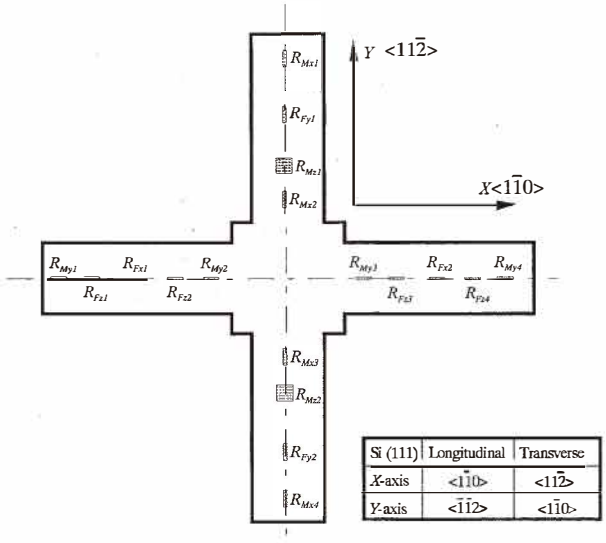

Accordingly, eqs. (15) and (16) simplify to:

$$\frac{\Delta R}{R} = \pi'_{11}\sigma_1 + \pi'_{12}\sigma_2 + \pi'_{13}\sigma_3 \approx \pi'_{11}\sigma_1, \tag{17}$$

$$\frac{V_{out}}{V_{in}} = \pi'_{66}\tau_6. \tag{18}$$

π'_{11} will be called the longitudinal piezoresistance coefficient, denoted as π_L, and π'_{66} can be called shear piezoresistance coefficient, designated as π_S.

For p-type piezoresistors, π_{11} and π_{12} are sufficiently small in comparison with π_{44} so that they can be neglected. Equations (17) and (18) are thus approximated as:

$$\pi_{L\langle 1\bar{1}0\rangle} = \pi_{L\langle 11\bar{2}\rangle} = \frac{1}{2}(\pi_{11} + \pi_{12} + \pi_{44}) \approx \frac{1}{2}\pi_{44},$$

$$\pi_{S\langle 1\bar{1}0\rangle} = \pi_{S\langle 11\bar{2}\rangle} = \frac{1}{3}(\pi_{11} - \pi_{12} + 2\pi_{44}) \approx \frac{2}{3}\pi_{44}.$$

Equations (17) and (18) are thus approximated as:

$$\frac{\Delta R}{R} = \pi_L\sigma_L = \frac{1}{2}\pi_{44}\sigma_1 = S_{gn}\sigma_1, \tag{19}$$

$$V_{out} = \pi_S\sigma_S = \frac{2}{3}\pi_{44}\tau_6 V_{in} = S_{gs}\tau_6 V_{in}, \tag{20}$$

$$S_{gn} = \frac{1}{2}\pi_{44} \text{ and } S_{gs} = \frac{2}{3}\pi_{44}. \tag{21}$$

where S_{gn} and S_{gs} are the stress sensitivities of the conventional and shear piezoresistors, respectively.

Table 1 summarizes increases and decreases of resistance of the normal piezoresistors and output voltages of the four-terminal piezoresistors due to the applied loads. The ' + ' and ' – ' signs indicate, respectively, an increase and decrease, ' 0 ' means unchanged and ' = ' means a similar change in both sign and magnitude in piezoresistors of a corresponding bridge. Shaded regions indicate where the response of the corresponding bridge is non-zero.

2.3 *Electrical circuits and working principle*

Based on Table 1, piezoresistors are connected to form the measurement circuits so that the sensor can detect six components of force and moment independently. The Wheatstone bridge is a useful circuit to convert a change in resistance to an output voltage. The general measurement circuit for measuring the five components, (*Fx*, *Fy*, *Fz*, *Mx*, and *My*), is

Table 1.
Resistance changes of normal piezoresistors and output voltages of shear piezoresistors.

	Fx-bridge		***Fy***-bridge		***Fz***-bridge				***My***-bridge				***Mx***-bridge				***Mz***-circuit	
	R_{Fx1}	R_{Fx2}	R_{Fy1}	R_{Fy2}	R_{Fz1}	R_{Fz2}	R_{Fz3}	R_{Fz4}	R_{My1}	R_{My2}	R_{My3}	R_{My4}	R_{Mx1}	R_{Mx2}	R_{Mx3}	R_{Mx4}	R_{Mz1}	R_{Mz2}
Fx	+	−	0	0	+	+	−	−	+	+	−	−	0	0	0	0	+	−
Fy	0	0	+	−	0	0	0	0	0	0	0	0	+	+	−	−	0	0
Fz	=	=	=	=	+	−	−	+	+	−	−	+	+	−	−	+	0	0
My	0	0	0	0	+	−	+	−	+	−	+	−	0	0	0	0	+	−
Mx	0	0	0	0	0	0	0	0	0	0	0	0	+	−	+	−	0	0
Mz	0	0	0	0	0	0	0	0	0	0	0	0	0	0	0	0	=	=

created by connecting in parallel five independent detecting potentiometer circuits together and with a common potentiometer circuit to form five Wheatstone bridges sharing a common half bridge (see Fig. 7(a)).

The resistances of the two resistors (R_C) of the common potentiometer circuit are identical and placed in a nonstress area. The output voltage of each bridge can be measured between the output point of each sensing potentiometer and the output point of the common one by the Wheatstone bridge rule to find the corresponding applied load. This circuit configuration also provides the best compensation for the temperature dependence of piezoresistors. The output voltage of each bridge can be written as below:[27]

$$V_{outFz} = \frac{1}{4}\left[\frac{\Delta R_{Fz1} + \Delta R_{Fz4}}{R_{Fz1} + R_{Fz4}} - \frac{\Delta R_{Fz2} + \Delta R_{Fz3}}{R_{Fz2} + R_{Fz3}}\right]V_{in}, \tag{22}$$

$$V_{outMx} = \frac{1}{4}\left[\frac{\Delta R_{Mx1} + \Delta R_{Mx3}}{R_{Mx1} + R_{Mx3}} - \frac{\Delta R_{Mx2} + \Delta R_{Mx4}}{R_{Mx2} + R_{Mx4}}\right]V_{in}, \tag{23}$$

$$V_{outMy} = \frac{1}{4}\left[\frac{\Delta R_{My1} + \Delta R_{My3}}{R_{My1} + R_{My3}} - \frac{\Delta R_{My2} + \Delta R_{My4}}{R_{My2} + R_{My4}}\right]V_{in}, \tag{24}$$

$$V_{outFx} = \frac{1}{4}\left[\frac{\Delta R_{Fx1}}{R_{Fx1}} - \frac{\Delta R_{Fx2}}{R_{Fx2}}\right]V_{in}, \tag{25}$$

$$V_{outFy} = \frac{1}{4}\left[\frac{\Delta R_{Fy1}}{R_{Fy1}} - \frac{\Delta R_{Fy2}}{R_{Fy2}}\right]V_{in}, \tag{26}$$

where V_{in} is the input voltage. Note that all conventional piezoresistors mentioned here are identical.

Two four-terminal piezoresistors for measuring the moment around the *Z*-axis can give the output voltage directly without any additional converting circuits (eq. (20)). These

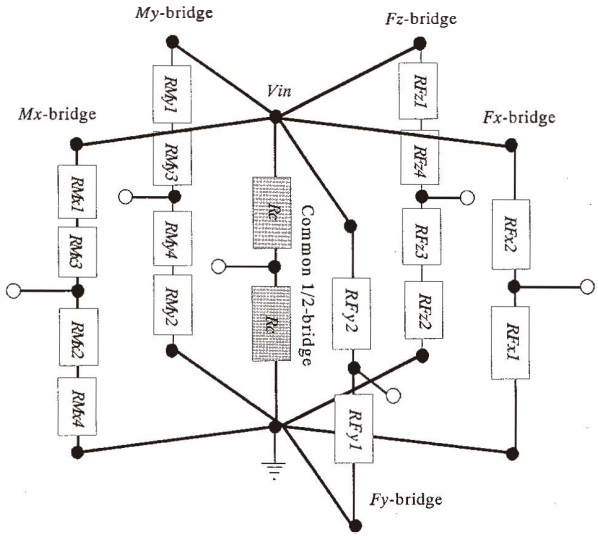

(a) Five Wheatstone bridges to measure *Fx, Fy, Fz, Mx* and *My*.

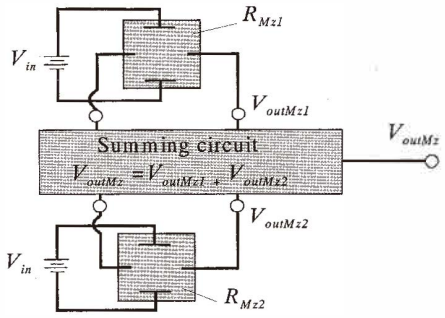

(b) Summing circuit to measure moment *Mz*.

Fig. 7. Measurement circuits.

piezoresistors are connected together via a standard operational amplifier to form a summing circuit,[27] which performs the algebraic addition operation between the voltages V_{outMz1} and V_{outMz2} of the two piezoresistors R_{Mz1} and R_{Mz2}, respectively (see Fig. 7 (b)).

$$V_{outMz} = V_{outMz1} + V_{outMz2}, \tag{27}$$

where V_{outMz1} and V_{outMz2} are calculated from eq. (20).

The next sub-sections will describe the working principle of the sensing chip.

2.3.1 *Detection of tangential forces Fx and Fy*

When a tangential force Fx in the X-direction is applied to the sensing chip, the beam ① with piezoresistor R_{Fx1} will be subjected to a tensile stress (Fig. 3(a)), while the opposite beam (beam ①), on which piezoresistor R_{Fx2} is located, will undergo a corresponding compression, hence $\Delta R_{Fx1} = -\Delta R_{Fx2}$. As a result, the output voltage of the Fx-bridge is nonzero, (see eq. (25)):

$$V_{outFx} = \frac{1}{2}\frac{\Delta R_{Fx1}}{R_{Fx1}} V_{in} = \frac{1}{4}\pi_{44}\sigma_1 V_{in}, \text{ and } S_{CFx} = \frac{\frac{V_{outFx}}{\Delta R_{Fx1}}}{R_{Fx1}} = \frac{V_{in}}{2}, \tag{28}$$

where S_{CFx} is defined as the circuit sensitivity of the Fx-bridge. By contrast, R_{Fy1} and R_{Fy2} in the Y-oriented beam exhibit no change in resistance because the longitudinal stresses in them are nearly equal to zero (Fig. 3 (b)). Therefore, the Fy-bridge is still balanced, *i.e.*, there is no response in this bridge (see eq. (26)). Similarly, the Mx-bridge has no response. In the case of the Fz-bridge, as the stresses at R_{Fz1} and R_{Fz4} have the same absolute magnitude, but are of opposite sign, so $\Delta R_{Fz1} = -\Delta R_{Fz4}$. Analogously, $\Delta R_{Fz2} = -\Delta R_{Fz3}$. Therefore $V_{outFz} = 0$, so the Fz-bridge has no sensitivity to the force Fx. Similarly, the My-bridge has no response. In the Y-oriented beam, shearing stresses with the same magnitude but opposite in sign will exist in four-terminal piezoresistors R_{Mz1} and R_{Mz2} (Fig. 3 (b)), so the total output voltage of the Mz-circuit is still zero (see eq. (27)). Note that four-terminal piezoresistors with crystal directions mentioned above are not sensitive to longitudinal stress (see eq. (20)).

The detection of tangential force Fy is similar to that of Fx.

2.3.2 *Detection of vertical force Fz*

When a vertical force Fz is applied to the sensing chip, from the FEM result, (Fig. 4), the longitudinal stresses in the four piezoresistors of the Fz-bridge can be written as below:

$$\sigma_{R_{Fz1}} = \sigma_{R_{Fz4}} = -\sigma_{R_{Fz2}} = -\sigma_{R_{Fz3}}$$

where $-\sigma_{R_{Fzi}}$ is the longitudinal stress at piezoresistor R_{Fzi}, $i = \overline{1,4}$. Therefore, $\Delta R_{Fz1} = \Delta R_{Fz4} = -\Delta R_{Fz2} = -\Delta R_{Fz3}$. Consequently, the Fz-bridge is unbalanced, and the output response is different from zero (see eq. (22)):

$$V_{outFz} = \frac{1}{2}\frac{\Delta R_{Fz1}}{R_{Fz1}} V_{in} = \frac{1}{4}\pi_{44}\sigma_1 V_{in} \text{ and } S_{CFz} = \frac{\frac{V_{outFz}}{\Delta R_{Fz1}}}{R_{Fz1}} = \frac{V_{in}}{2}, \tag{29}$$

where S_{CFx} is defined as the circuit sensitivity of the Fz-bridge. Due to the symmetry of the arrangement of piezoresistors and the structure of the sensing chip, the logitudinal stresses at R_{Fx1} and R_{Fx2} are equal (Fig. 4), hence their resistance changes are equal: ΔR_{Fx1}=ΔR_{Fx2}, so

the output voltage of the *Fx*-bridge is equal to zero (see eq. (25)). Similarly, no response will occur in the *Fy*-bridge. Likewise, in the case of the *Mx*-bridge, the total resistance change of the upper arm ($\Delta R_{My1}+\Delta R_{My3}$) is equal to that of the lower arm ($\Delta R_{My2}+\Delta R_{My4}$), (Fig. 7 (a)); therefore the *My*-bridge is still balanced. Similarly, the response of the *Mx*-bridge is zero. The in-plane shear stress component is equal to zero at R_{Mz1} and R_{Mz2}, so the output of the *Mz*-circuit is equal to zero.

2.3.3 *Detection of moments Mx and My*

When a moment *My* around the *Y*-axis is applied to the sensing chip, as can be seen from the FEM result (see Fig. 2 (a)), the normal stresses in the four piezoresistors of the *My*-bridge can be written as $\sigma_{R_{My1}} = -\sigma_{R_{My4}} = -\alpha\sigma_{R_{My2}} = \alpha\sigma_{R_{My3}}$, where α is a constant depending upon the width and length of the beam; in this study, $\alpha \approx 0.75$. Therefore, the resistance change in the *My*-bridge can be written by $\Delta R_{My1} = -\Delta R_{My4} = -\alpha\Delta R_{My2} = \alpha\Delta R_{My3}$. Substituting this relation into eq. (24), the output voltage and circuit sensitivity of the *My*-bridge are expressed by:

$$V_{outMy} = \frac{1}{4}\frac{(1+\alpha)\Delta R_{My3}}{R_{My3}} V_{in} = \frac{1}{8}(1+\alpha)\pi_{44}\sigma_1 V_{in} \text{ and } S_{CMy} = \frac{(1+\alpha)V_{in}}{4}. \tag{30}$$

However, for the piezoresistors of the *Fz*-bridge, $\Delta R_{Fz1} = -\Delta R_{Fz4}$ and $\Delta R_{Fz2} = -\Delta R_{Fz3}$. Therefore, the output voltage of the *Fz*-bridge is zero, (see eq. (22)). R_{Fx1} and R_{Fx2} are intentionally located at the positions where the normal stress, induced by the concentrated moment *My*, is equal to zero, as mentioned in section 2.2. As a result, the *Fx*-bridge has no response either. The FEM analysis result has shown that these positions are unchanged when the beam thickness and/or the moment *My* are changed. In the *Y*-axial beam, the longitudinal stress is equal to zero along the central longitudinal axis (or at the piezoresistors), so the *Fy*-bridge and *Mx*-bridge have no response. Shearing stresses of identical magnitude but opposite sign exist along the *Y*-axial beams, therefore they also exist in the four-terminal piezoresistors R_{Mz1} and R_{Mz2}, (Fig. 2 (b)), so the total output voltage of the *Mz*-circuit is still zero, (eq. (27)).

The detection of moment *Mx* is analogous to *My*.

2.3.4 *Detection of moment Mz*

When a moment around the *Z*-axis *Mz* is applied to the sensing chip, only shearing stresses exist in the piezoresistors (Fig. 5). These stresses are equal in magnitude and sign at R_{Mz1} and R_{Mz2}, so the total output voltage in the *Mz*-circuit is nonzero:

$$V_{outMz} = 2V_{outMz1} = 2S_{gs}\tau_s V_{in} = \frac{2}{3}\pi_{44}\tau_6 S_{CMz}, \tag{31}$$

where $S_{CMz} = 2V_{in}$ is the circuit sensitivity of the *Mz*-bridge. The other bridges have no response to these shearing stresses.

3. Fabrication Process

The sensing chip was fabricated by micromachining processes described briefly by the following steps (see Fig. 8):

Step 1: The starting material was a 4-inch n-type (111) silicon wafer with a thickness of 400 μm.

Step 2: A 0.3 μm-thick SiO_2 insulator layer was formed by a thermal oxidization process.

Step 3: Piezoresistors were patterned so that their principal axes align with the crystal directions $<1\bar{1}0>$ and $<11\bar{2}>$. Boron ions were diffused to form p-type piezoresistors by using a spin-on diffusion source (PBF, Tokyo Ohka Kogyo Co., Ltd). A pre-deposition process was performed in N_2 at 1000°C for 60 min. Then, a drive-in process was carried out in dry O_2 at 1100°C for 30 min to activate boron ions in the Si. In order to reduce the temperature sensitivity of piezoresistors, the surface impurity concentration was controlled at about 5×10^{19} cm^{-3}.

Step 4: Contact holes were opened by wet etching in buffered HF solution.

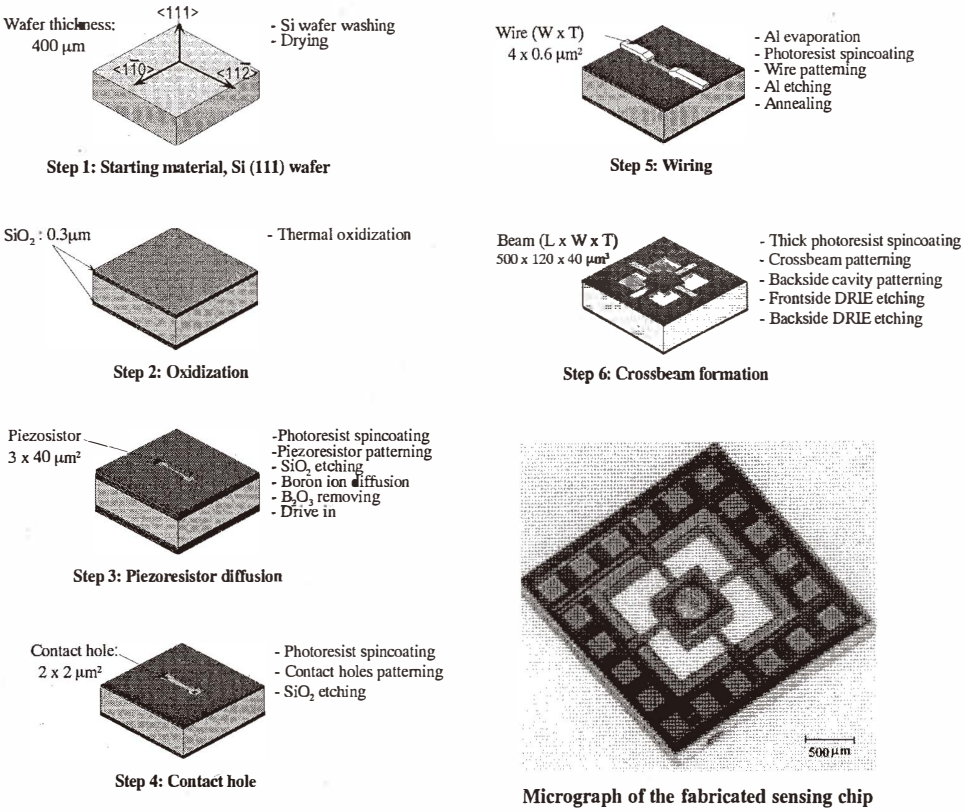

Fig. 8. Fabrication process for sensing chip.

Step 5: 0.6-μm-thick aluminum wires and bonding pads were formed by vacuum evaporation, photolithography, and etching processes. Next, a sintering process was performed in N_2 at 400°C for 30 min to form an Ohmic contact between electrodes and piezoresistors.
Step 6: A crossbeam pattern was defined by photolithography using a double-sided mask aligner. Then, a front side surface deep reactive ion etching (D-RIE) process was performed to a depth of 40 μm. Finally, the cavity and overload-stopper were formed by D-RIE from the back surface. A thick photoresist was adopted as a passivation layer during the D-RIE process.

4. Calibration

Calibration of the sensing chip was performed using an ultra small load indenter (Shimadzu Co., DUH201), controlled by a computer to generate a precise force for the calibration.

The force *Fz* was calibrated by applying the indenter directly to the center of the sensing chip (Fig. 9(a)).

To calibrate the moments *My*, the calibration force *F* was applied at a point 350 μm

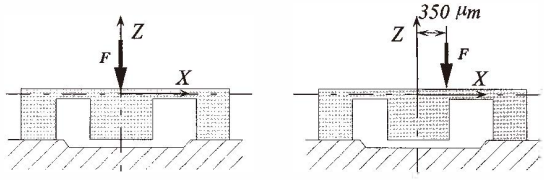

(a) *Fz* calibration (b) *My* (or *Mx*) calibration

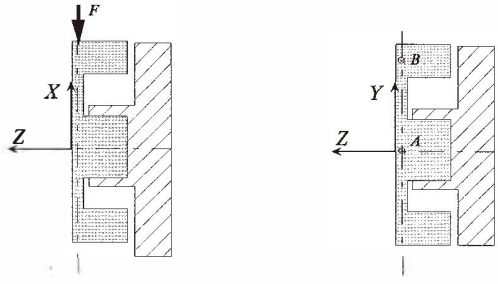

(c) *Fx* (or *Fy*) and *Mz* calibration. Right-hand side figure is the top-view of the left-hand side one. Force *F* is applied to point *A* in *Fx* calibration, and to point *B* in *Mz* calibration.

Fig. 9. Schematic views of the mounting of the chip for calibration.

away from the center of the chip on the central line of the *X*-oriented beam (Fig. 9(b)). Consequently, a force *Fz* (same magnitude with force *F*), and a moment *My* (whose value is the product of $F \times 350$ μm), were generated at the center of the central plate of the chip. The calibration results have confirmed that these components (*Fz* and *My*) were detected separately. The moment *Mx* was calibrated similarly to *My*.

For calibration of *Fx* and *Fy*, the central block of the chip was mounted onto a base as shown in Fig. 9(c), and calibration force *F* from the indenter was applied directly to point *A* on the edge surface of the chip. Finally, to calibrate the moment *Mz*, we used the same configuration as for *Fx* calibration, but the calibration force *F* was applied at point *B*, 1500 μm away from point *A* (Fig. 9(c)). As a result, a tangential force *Fx* of the same magnitude and direction as *F*, and a moment *Mz*, whose magnitude is the product of *F* and the distance from point *A* to point *B*, is produced. The calibration results have confirmed that these components (*Fx* and *Mz*) were detected separately.

Figure 10 shows the calibration results of six components of force and moment (input voltage: 5 V, temperature: 25°C). The theoretical outputs (calculated based on FEM, book values of piezoresistive coefficients,[23] and circuit sensitivities, eqs. (28)–(31)) are also displayed in this figure for reference. A good agreement between the design and experimental values was obtained. The sensitivities of each components are: $S_{Fz} = 1.32$ mV/mN, $S_{Fx} = 0.12$ mV/mN, $S_{Fy} = 0.107$ mV/mN, $S_{Mx} = 4$ mV/mNμm, $S_{My} = 3.88 \times 10^{-3}$ mV/mNμm, and $S_{Mz} = 4.6 \times 10^{-4}$ mV/mNμm. The crosstalk was small. Maximum crosstalk of 4% was

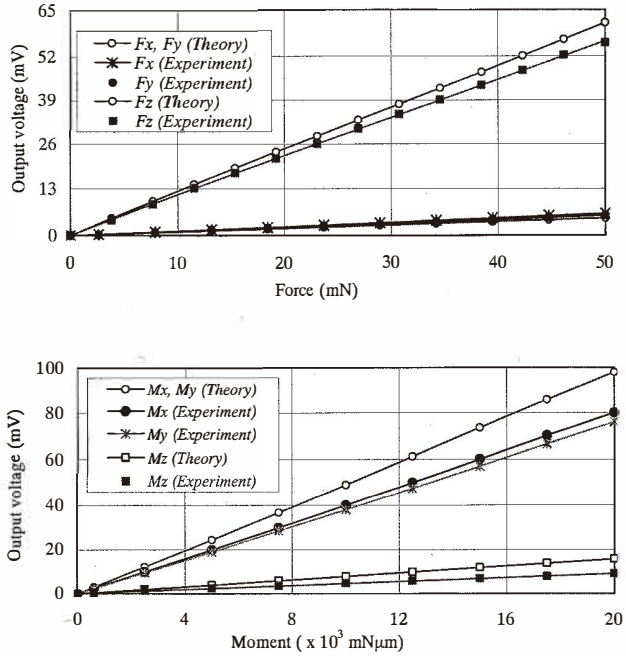

Fig. 10. Calibration result: output voltages versus applied loads.

measured. The maximum nonlinearities (NL) of each of the components are $NL_{Fx} = NL_{Fy} =$ 1.02%F.S., NL_{Fz} = 0.53% F.S., $NL_{Mx} = NL_{My}$ = 2.51%F.S., and NL_{Mz} = 1.62%F.S. The relationship of the output voltages of measurement circuits and the applied force and moment components can be summarized as below:

$$\begin{bmatrix} V_{Fx} \\ V_{Fy} \\ V_{Fz} \\ V_{Mx} \\ V_{My} \\ V_{Mz} \end{bmatrix} = \begin{bmatrix} 0.121 & 0.0035 & 0.007 & 0.042 & 0.009 & 0.008 \\ 0.0041 & 0.107 & 0.003 & 0.024 & 0.025 & 0.002 \\ 0.0022 & 0.0035 & 1.32 & 0.031 & 0.024 & -0.002 \\ 0.0021 & 0.0040 & 0.022 & 4.00 & 0.029 & 0.007 \\ 0.0025 & 0.0042 & 0.01 & 0.039 & 3.88 & 0.011 \\ 0.0023 & 0.0032 & 0.008 & 0.005 & 0.036 & 0.461 \end{bmatrix} \begin{bmatrix} Fx \\ Fy \\ Fz \\ Mx \\ My \\ Mz \end{bmatrix} \quad (32)$$

where the unit of force is mN, that of moment is NMm and the output voltage is mV. The range of forces Fx and Fy is 1000 mN, that of force Fz is 100 mN, that of moments Mx and My is 30 Nμm, and that of moment Mz is 300 Nμm.

In eq. (32), the off-diagonal components, which represent the crosstalks, were not zero. The crosstalks occurred due to some defects in the fabrication process, such as misalignments of piezoresistors on the beams. As described in section 2.2, the piezoresistors to measure one specific component of force or moment are laid out symmetrically through the central point O. The misalignment could break this symmetric feature, and causes undesirable unbalances in the Wheatstone bridges. Consequently, slight crosstalk can occur. A well-controlled fabrication process can improve this situation.

5. Application in Turbulent Flow Measurement

One of the holy grails in geophysical research is reliable simulation technology for the micromechanics of sediment particle erosion and transport, the fundamental processes shaping the land and major contributors to flooding phenomena. In this context, the immediate purpose of this sensor is to measure the fluctuating components of force and moment on a particle at the bed of a turbulent channel flow. Introducing the present sensor in such experiments, we will investigate the spatio-temporal relationship between near-wall vortices and particles for the purpose of advancing sediment transport simulations. The configuration of this sensor is shown in Fig. 11. The 6-DOF force-moment sensing chip is located inside a test particle so that its centroid coincides with the center of the surface of the sensing chip. The test particle has a diameter of about 8 mm and is made of polyethylene, of which the specific gravity is 0.965, nearly equal to that of water. By selection of this material, the vertical force component (buoyancy force) from water acting on the particle is almost eliminated during operation. 25-μm-diameter gold wires connecting the sensing chip to the off-chip circuits are isolated and fixed on the surfaces of a base pillar. The sensing chip is completely overload-protected by a protection base located under it. All electrical elements of the sensor are waterproofed by a silicone rubber layer. Forces and/or moments from the liquid flow acting on the test particle will be transmitted

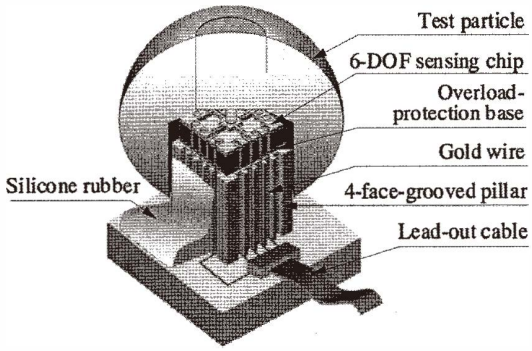

Fig. 11. Configuration of a turbulent flow sensor.

to the sensing chip via a force transmission pillar placed at the center of the sensing chip. Consequently, the sensing areas will be deformed and the resistance of the piezoresistors will change, thus changing the output of the corresponding bridge circuits.

Figure 12 shows the sensor working in a water flow channel. The flow velocity was measured directly at a point in front of the sensor by LDV (laser Doppler velocimetry). Figure 13 shows a result of a combined experiment of the flow sensor and LDV system (input voltage is $Vin = 2$ V). The output voltages of the sensor (V_{My} and V_{Fz}, lower graph) and flow velocity measured by LDV (upper graph) are shown versus experimental time. Water flow in this experiment was controlled so that the flow velocity was reduced gradually from 50 cm/s to 10 cm/s. Good agreement between the sensor output and LDV results was obtained. This preliminary result confirms that the designed sensitivities of the sensing chip were appropriate to measure forces and moments acting on particles in a turbulent flow. More carefully controlled experiments in water flow are being performed, and the results will be compared with those of simulation.

6. Conclusions

The theoretical investigation, design, fabrication, and calibration of a 6-DOF force-moment sensing chip have been presented. By combining normal and shear piezoresistors in Si (111), and arranging and connecting them appropriately, their number was considerably reduced in comparison with the prior 6-DOF piezoresistive force sensors known to the authors; consequently, the sensing chip is smaller, more sensitive, and consumes less power. Calibration for six components of force versus output voltages has been completed. The sensitivities are high, linear, and close to the design values. The crosstalks are smaller than that of previously reported 6-DOF micro force moment sensors.

One specific application of the sensing chip to measure forces and moments acting on a test particle in a turbulent flow is now being carried out, and preliminary measurement results have been obtained and are being analyzed. The sensitivities are sufficiently high to measure the forces and moments expected to act on particles in the slow flows of interest in our research.

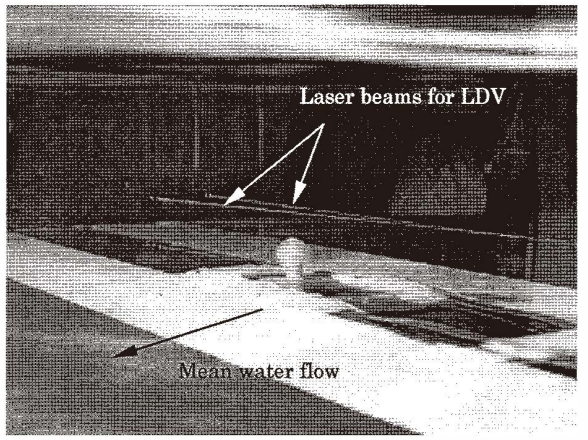

Fig. 12. Sensor is operating in a water channel.

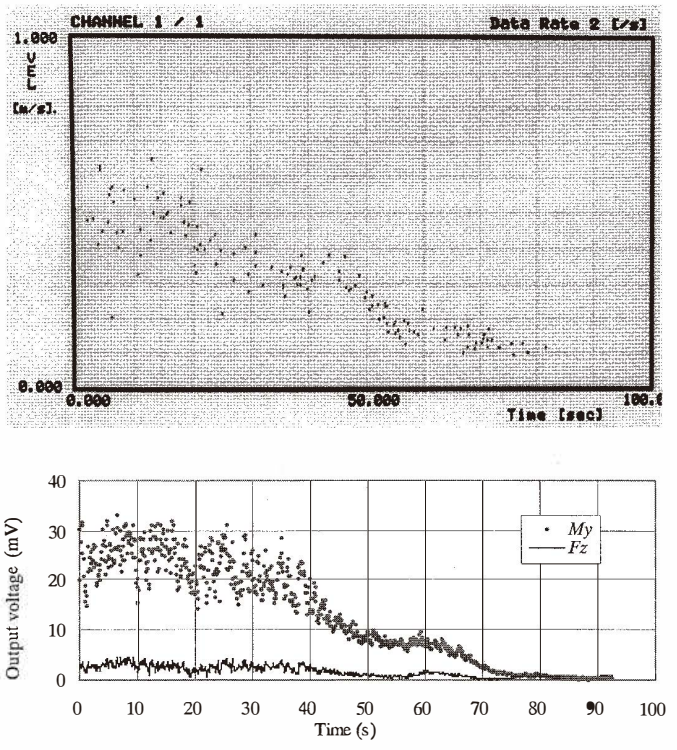

Fig. 13. Combined experiment of sensor and LDV (input voltage *Vin* = 2 V).

The design of the sensing chip presented above can be applied to other integrated force-based micro devices, such as tactile sensors, and micro multi-axis accelerometers.

Acknowledgement

This research has been supported in part by grants from the "Science frontier projects II" of Japanese Government. The authors wish to thank Professor Y. Isono and the members of Micro Nano Mechanical Laboratory, Ritsumeikan University, Japan, for their enthusiastic help during calibration of the sensor. We are also grateful to Messrs. T. A. Nguyen and V. C. Nguyen for assistance with the turbulent flow experiments.

References

1 L. Wang and D. J. Beebe: Sensors and Actuators A **84** (2000) 33.
2 W. L. Jin and C. D. Mote: Sensors and Actuators A **65** (1998) 88.
3 D. J. Beebe, A. S. Hsieh and R. G. Radwin: Sensors and Actuators A **50** (1995) 55.
4 F. Jiang, Y. Tai, K. Walsh, T. Tsao, B. Lee and C. Ho: Proc. IEEE MEMS 1997 (IEEE, Nagoya, 1997) p. 465.
5 T. Mei, L. Wen, G. Yu, C. Yong, N. Lin and C. M. Ho: Sensors and Actuators A **80** (2000) 155.
6 C. T. Yao, M. C. Peckerar, J. H. Wasilik, C. Amazeen and S. Bishop: Proc. IEEE Micro Robots and Teleoperators Workshop (1987).
7 R. A. Grahn: US Patents No. RE37065, 2001.
8 F. W. Sinden and R. A. Boie: IEEE Robot Conference Proc. (IEEE,1986) p.1806.
9 K. Ogata: Measuring Technology, No. 11, Vol.15, Japan, 1987.
10 C. G. Kang: Sensors and Actuators A **90** (2001) 31.
11 G. S Kim, D. I Kang and S. H. Rhee: Sensors and Actuators A **77** (1999) 209.
12 K. Okada: Technical Digest of The 9th Sensor Symposium (IEEJ, Japan, 1990) p. 245.
13 W. L. Jin and C. D. Mote: Sensors and Actuators A **65** (1998) 109.
14 T. Sarpkaya: ASME Journal of Applied Mechanics **85** (1963) 13.
15 D. Hall: Journal of Fluid Mechanics, Vol. **187** (1988) 451.
16 T. Von Papen, H. D. Ngo, E. Obermeier, M. Schober, S. Pirskawetz and H. H. Fernholz: Transducer 2001 (Springer, Munich, 2001) p. 1476.
17 S. M. Kumar, W. C. Reynolds and T. W. Kenny: IEEE MEMS Conference (IEEE, Orlando, 1999) p.135.
18 T. Toriyama and S. Sugiyama: Journal of Micro Electromechanical Systems Vol. 11, No. 5, (2002).
19 T. Toriyama and S. Sugiyama: Journal of Applied Physics **81** (2002) 2797.
20 W. G. Pfann and R. N. Thurston: Journal of Applied Physics **32** (1961) 2008.
21 W. P. Mason and R. N. Thurston: Journal of the Acoustical Society of America, Vol. 29, No. 10, (1957) 1096.
22 C. S. Smith: Physical Rev. **94** (1954) 42.
23 O. N. Tufte and E. L. Stelzer: Journal of Applied Physics **34** (1962) 313.
24 Y. Kanda: Japanese Journal of Applied Physics **26** (1987) 1031.
25 J. J. Wortman and R. A. Evans: Journal of Applied Physics **36** (1965) 153.
26 S. Timosenko: Strength of Materials, 3rd Edition, Part I (Van Nostrand Reinhold Company, USA, 1955) Chaps. I, IV and X.
27 W. D. James, F. R. William and G. Kenneth: Instrumentation For Engineering Measurements (John Wiley & Sons, USA, 1984) Chaps. IV and VI.